

# EGGS: Edge Guided Gaussian Splatting for Radiance Fields

Yuanhao Gong

gong@szu.edu.cn

Electronics and Information Engineering, Shenzhen University, China

## ABSTRACT

The Gaussian splatting methods are getting popular. However, their loss function only contains the  $\ell_1$  norm and the structural similarity between the rendered and input images, without considering the edges in these images. It is well-known that the edges in an image provide important information. Therefore, in this paper, we propose an Edge Guided Gaussian Splatting (EGGS) method that leverages the edges in the input images. More specifically, we give the edge region a higher weight than the flat region. With such edge guidance, the resulting Gaussian particles focus more on the edges instead of the flat regions. Moreover, such edge guidance does not create the computation cost during the training and rendering stage. The experiments confirm that such simple edge-weighted loss function indeed improves about 1 ~ 2 dB on several difference data sets. With simply plugging in the edge guidance, the proposed method can improve all Gaussian splatting methods in different scenarios, such as human head modeling, building 3D reconstruction, etc.

## CCS CONCEPTS

• Computing methodologies → Neural networks.

## KEYWORDS

Gaussian, splatting, edge, guided, radiance

### ACM Reference Format:

Yuanhao Gong. 2018. EGGS: Edge Guided Gaussian Splatting for Radiance Fields. In *Proceedings of Make sure to enter the correct conference title from your rights confirmation email (Conference acronym 'XX)*. ACM, New York, NY, USA, 5 pages. <https://doi.org/XXXXXXX.XXXXXXX>

## 1 INTRODUCTION

Getting 3D signals from multi-view images is a key task in the wide-reaching field of computer vision. It involves the intricate job of examining and interpreting the varying viewpoints presented by the array of images, all to build a precise 3D representation of the subject. This core task underpins a host of applications and studies in computer vision, making it a crucial area to grasp and comprehend.

The challenge here is to understand depth and perspective from two-dimensional images, which is not an easy task. It's more than just viewing images - it's about turning flat visuals into a three-dimensional perspective. This involves advanced math techniques

Permission to make digital or hard copies of all or part of this work for personal or classroom use is granted without fee provided that copies are not made or distributed for profit or commercial advantage and that copies bear this notice and the full citation on the first page. Copyrights for components of this work owned by others than ACM must be honored. Abstracting with credit is permitted. To copy otherwise, or republish, to post on servers or to redistribute to lists, requires prior specific permission and/or a fee. Request permissions from [permissions@acm.org](mailto:permissions@acm.org).  
Conference acronym 'XX, June 03–05, 2018, Woodstock, NY

© 2018 Association for Computing Machinery.  
ACM ISBN 978-1-4503-XXXX-X/18/06...\$15.00  
<https://doi.org/XXXXXXX.XXXXXXX>

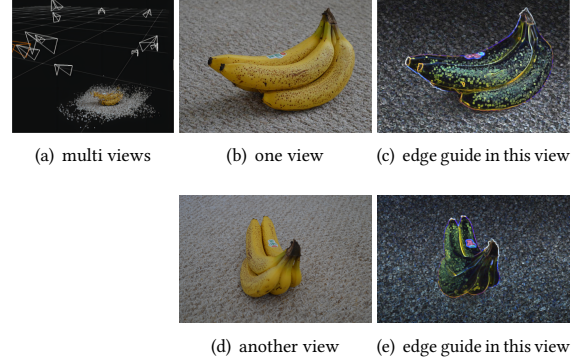


**Figure 1: The edge guide in each view image can force more particles on the edge region, improving the scene accuracy.**

that are complex and sophisticated. Strong algorithms are also needed to manage this translation process. They need to interpret and analyze data quickly and accurately. On top of that, we need significant computational power to process the large amount of data and operations. This makes the task complex and challenging, but also quite interesting from a technical perspective.

NeRF, which stands for Neural Radiance Fields, represents a groundbreaking and innovative method in the field of 3D modelling. It employs the use of a fully connected deep network, a complex and intricate system, to model the volumetric scene function. This function is integral to creating a realistic and immersive 3D environment. What sets NeRF apart is its ability to generate high-quality, novel views of 3D scenes. This is achieved from sparse input views, meaning that even with limited input data, the system can produce detailed and comprehensive 3D scene representations. This illustrates the power and potential of the NeRF method in transforming the way we approach and utilize 3D modelling technology.

Recently, 3D Gaussian splatting has gained quite a bit of traction [27]. It's a key player in scene estimation and rendering jobs. It uses the Gaussian distribution to figure out the scene's properties, and then uses this information to create detailed and precise illustrations. It avoids the ray tracing in the NeRF methods. Instead, it uses splatting for the image rendering. This method has been a big step in pushing 3D graphics forward.

### 1.1 Particle Representation

For a 3D signal  $f(\vec{x})$ , where  $\vec{x}$  is the spatial coordinate, it can be expressed as a convolution operation with the classical Dirac delta function

$$f(\vec{x}) = \int f(\vec{\tau})\delta(\vec{x} - \vec{\tau})d\vec{\tau}. \quad (1)$$

Although this is exact, the abstract delta function is not computationally practical.

To improve the computation property, the above equation is relaxed into the follow discrete expression

$$\hat{f}(\vec{x}) \equiv \sum_{k=1}^K f(\vec{\tau}_k) W(\vec{x} - \vec{\tau}_k, h_k) V_k, \quad (2)$$

where  $\hat{f}$  is the reconstructed signal from this discrete representation,  $K$  is the total number of particles,  $k$  is the particle index,  $W$  is a particle kernel function,  $h_k$  is the kernel parameter, and  $V_k$  is the volume of the particle.

In most of cases, the multiplication value  $f(\vec{\tau}_k) V_k$  can be treated as one variable  $A_k$  for convenience reason, leading to the following particle representation

$$\hat{f}(\vec{x}) \equiv \sum_{k=1}^K A_k W(\vec{x} - \vec{\tau}_k, h_k). \quad (3)$$

The introduced  $A_k$  can carry multiple features, such as mass, temperature, curvature, etc. It is generic for the particle representation.

With such particle representation, we can evaluate the distance between the original signal  $f(\vec{x})$  and its reconstruction from the particle representation. More specifically, the distance is

$$L(f, \hat{f}) = \frac{1}{2} \|f(\vec{x}) - \hat{f}(\vec{x})\|_2^2. \quad (4)$$

One important property of particle representation is that this distance can be reduced if more particles are added. This property makes the particle representation flexible and compact.

The gradients of the particle representation with respect to the spatial coordinate, the parameter  $h_k$  and  $\vec{\tau}_k$  are

$$\frac{\partial L}{\partial \vec{x}} = (\hat{f} - f) \sum_{k=1}^K A_k \frac{\partial W(\vec{x} - \vec{\tau}_k, h_k)}{\partial \vec{x}}, \quad (5)$$

$$\frac{\partial L}{\partial h_k} = (\hat{f} - f) \sum_{k=1}^K A_k \frac{\partial W(\vec{x} - \vec{\tau}_k, h_k)}{\partial h_k}, \quad (6)$$

$$\frac{\partial L}{\partial \vec{\tau}} = (\hat{f} - f) \sum_{k=1}^K A_k \frac{\partial W(\vec{x} - \vec{\tau}_k, h_k)}{\partial \vec{\tau}}. \quad (7)$$

These gradients can be used to update the center and shape parameters of the particles.

## 1.2 3D Gaussian Splatting

The 3D Gaussian splatting (3DGS) method and its variants are special cases of the particle representation. More specifically, the 3D Gaussian splatting uses the anisotropic Gaussian kernels in the particle representation

$$\hat{f}(\vec{x}) = \sum_{k=1}^K A_k G(\vec{\tau}_k, \Sigma_k), \quad (8)$$

$$\text{where } G(\vec{\tau}_k, \Sigma_k) = \exp[-(\vec{x} - \vec{\tau}_k)^T \Sigma_k^{-1} (\vec{x} - \vec{\tau}_k)]. \quad (9)$$

The non negative covariance matrix is  $\Sigma = RSS^T R^T$ , where  $S$  is a diagonal scaling matrix and  $R$  is a rotation matrix.

This 3D Gaussian particle is then splatted on the the 2D image plane. The covariance in 2D is computed via

$$\Sigma^{2D} = JW\Sigma W^T J^T, \quad (10)$$

where  $W$  is the world-to-camera matrix and  $J$  is a local matrix for the projection.

The color  $c(u, v)$  at a view is then defined via an alpha blending

$$c(u, v) = \sum_{k=1}^K c_k \alpha_k G_k^{2D} \prod_{j=1}^{k-1} (1 - \alpha_j G_j^{2D}), \quad (11)$$

where  $c_k$  is a view dependent color,  $\alpha_k$  is the transparency,  $G^{2D}$  is a 2D Gaussian function with the covariance matrix  $\Sigma^{2D}$  in Eq. (10). And  $k$  is sorted from the view direction. The coordinate  $(u, v)$  indicates the image space coordinate.

The rendered image  $c(u, v)$  is then compared with the observed image  $im$  via a  $\ell_1$  distance and the structural similarity distance

$$\text{Loss}(c, im) = (1 - \lambda)|c - im| + \lambda D_{SSIM}(c, im), \quad (12)$$

where  $\lambda > 0$  is a weight parameter and  $D_{SSIM}$  is a distance measurement using  $SSIM$ .

## 1.3 Variants of Gaussian Splatting

Thanks to the splatting, the Gaussian splatting methods do not need the ray tracing to render the observed image at a given view. As a result, these methods are much faster than the Nerf based approaches that require the ray tracing to perform the image rendering.

With the advantages of computational efficiency and the resulting high quality rendered images, various Gaussian splatting methods have been developed. For example, it can be applied in street modeling [34], human head modeling [32, 40] and human body modeling [1]. In [23], isotropic Gaussian function is adopted to reduce the orientation issue. And A compression method is developed to remove the unimportant Gaussian particles, reducing the file size [4, 28]. When we are writing this paper, 2D Gaussian splatting method is developed in [25], where 2D disks are attached to a surface. Similar idea is also shown in [24]. This method is more suitable for surface representation instead of volume representation. A survey on 3D Gaussian splatting can be found in [2].

## 1.4 Our Motivation and Contributions

Different from previous work that focuses on a specific field, we notice that the loss function treats each pixel equally. However, it is well-known that the edges in the image are more important than the flat region. This motivates us to develop an edge guided loss function. Our contributions are

- we introduce the edge guidance for the Gaussian splatting method.
- the edge guidance is generic and various edge functions can be adopted.
- we valid the effectiveness of the edge guidance via several numerical experiments.

## 2 EDGE GUIDED GAUSSIAN SPLATTING

In the loss function Eq. (12), the pixels at edges and the pixels at flat regions have the same weight. Therefore, these two types of pixels have the same influence on the result. However, we know that the edge information is more important in the human vision perception. It is reasonable to increase the weight for pixels at edges. This motivates us to develop an edge guided Gaussian splatting method, which achieves better results.

## 2.1 Edge Guidance

There are many different edge indicators, such as the classical gradient, Laplacian of Gaussian and Canny detector. These methods can be efficiently evaluated, although the accuracy may not achieve the state-of-the-art. Thanks to the efficiency, they can be deployed in real-time applications.

The edges can also be found by deep neural networks, such as [29, 30, 33]. Thanks to the powerful neural networks, these methods can get a higher accuracy in edge detection. Although the accuracy is satisfying, these methods require a large amount of computation resource, such as memory and high performance GPUs. This limits their deployment in practical applications. A survey about edge detection can be found in [26].

In this paper, we use a gradient based edge indicator function. More specifically, we define

$$\phi(u, v) = 1 + \beta \|\nabla im(u, v)\|_p, \quad (13)$$

where  $\beta > 0$  is a scalar parameter,  $\nabla$  is the gradient operator,  $p = \{1, 2\}$  indicates the standard  $\ell_1$  or  $\ell_2$  norm. The parameter  $\beta$  controls the gradient influence. If  $\beta = 0$ , then  $\phi = 1$  and this becomes the original Gaussian splatting method. At the flat region,  $\|\nabla im\| \approx 0$ ,  $\phi \approx 1$ . At the edges,  $\|\nabla im\| \gg 0$ , leading to  $\phi \gg 1$ . Therefore, this weight function will force Gaussian splatting to have a higher accuracy at the edges, which provides more visual information. One example of this weight function is shown in Fig. 1, where the values are linearly scaled for better visualization.

## 2.2 Our Loss Function

We impose the above weight function into the loss function, leading to the edge guided loss that is

$$Loss(c, im) = (1 - \lambda) \|\phi(u, v)(c - im)\|_1 + \lambda D_{SSIM}(c, im). \quad (14)$$

The proposed loss function has several advantages. First, the weight function  $\phi(u, v)$  is very generic and other edge indicating functions can also be adopted without changing the pipeline of the proposed method.

Second, the weight function is only determined by the observed input images. It is independent from the 3D radiance field. It works in the image space rather than in the 3D object space. Therefore, it can be pre-computed without estimating the unknown 3D signal. In contrast, some previous methods such as [3, 25] also use regularization on the estimated radiance field, for example, the smoothness of the signal or the normal consistency of the surface. Such smoothness relies on the estimated signal or surface, which has to be updated every step during the training process.

Third, the weight function does not increase the computation cost. Its computational performance is exactly the same as the original 3DGS. In other words, the proposed method does not increase the computation cost, but can improve the accuracy of the radiance field. The proposed method is a Gaussian splatting method with edge guidance. Thus, we name this method as edge guided Gaussian splatting (EGGS).

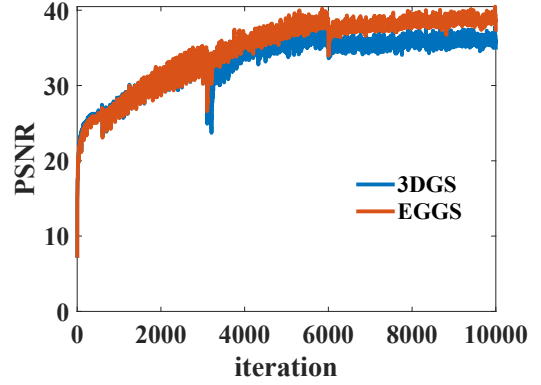


Figure 2: The PSNR during the training process (the lines are smoothed for better visualization). The blue line is 3DGS and the red line is EGGS. The EGGS can achieve better PSNR.

## 2.3 Others

The optimization and rendering in the proposed EGGS are exactly the same as the original 3DGS. We use the same splitting, merging and deleting strategy as the 3DGS. The only difference is the proposed edge guidance in the loss function.

## 3 EXPERIMENTS

With the simple edge guidance defined in Eq. (13) and the corresponding loss function in Eq. (14), we can optimize the Gaussian particles to obtain the scene representation. We test the proposed EGGS on three different data sets and compared the results with the counterpart from the 3DGS method.

### 3.1 Banana Dataset

The banana data set contains 16 images at different views. And each image has the  $3008 \times 2000$  resolution. Such high resolution can capture the details in the scene and improve the quality of the radiance field. We use 3DGS and EGGS to perform the reconstruction. The results are shown in Fig. 2 and 3.

In Fig. 2, we compared the 3DGS (blue line) and EGGS (red line) on this data set. The largest PSNR for 3DGS is about 41.7dB. In contrast, EGGS can achieve 43.8dB, which is about 2.1dB improvement. Such improvement is a big step to improve the radiance field. Be aware that such improvement is only caused by the edge guidance.

We visually show the results in Fig. 3, where the left column is for 3DGS and the right is for EGGS. It can be confirmed that EGGS has sharper edges and is much clearer. The letters in the red region are blurred in the 3DGS result and almost invisible. In the EGGS result, these letters can be roughly seen. In the bottom row, we show the RGB images with the Gaussian particle centers (indicated by the blue dots). In 3DGS, the dots are more uniform distributed. In EGGS, the dots are aligned with the edges. Such behavior confirms that the proposed edge guidance indeed forces the Gaussian particle to be aligned with the edges.

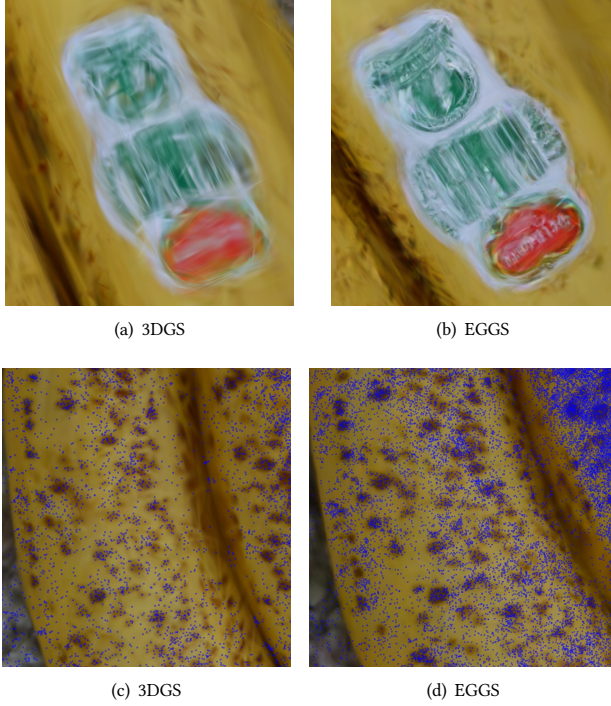


Figure 3: The detailed difference between 3DGS and EGGS on the banana data set. The top row shows that the edges in the EGGS are much clearer than the edges in 3DGS. The bottom row shows that EGGS puts more particles near the edges.

### 3.2 Train Dataset and Truck Dataset

The train data set contains 301 images, which have the  $980 \times 545$  resolution. One example input image is shown in Fig. 4(a), along with its edge guidance in Fig. 4(b). The train process is shown in Fig. 5 for the 10k iterations. Although it is not the converged state, we can still tell that the edge guidance indeed helps in improving the quality of the estimated radian field. The best PSNR for 3DGS and EGGS on this data set is 28.0 and 29.2, respectively. The improvement is about 1.2dB.

The truck data set contains 251 images, which have the  $979 \times 546$  resolution. One example input image is shown in Fig. 4(c), along with its edge guidance in Fig. 4(d). It shows similar behavior as previous data sets. And thus the training curves are omitted here. The best PSNR for 3DGS and EGGS on this data set is 28.4 and 29.5, respectively. The improvement is about 1.1dB.

These experiment results confirm that the proposed edge guidance indeed can improve the accuracy of the radiance field that is represented by 3DGS. The PSNR gain might depend on the scene.

### 3.3 PSNR Improvement

The PSNR improvements on these data sets are summarized in Table 1. In general, the edge guidance can improve the accuracy of the Gaussian particle representation.

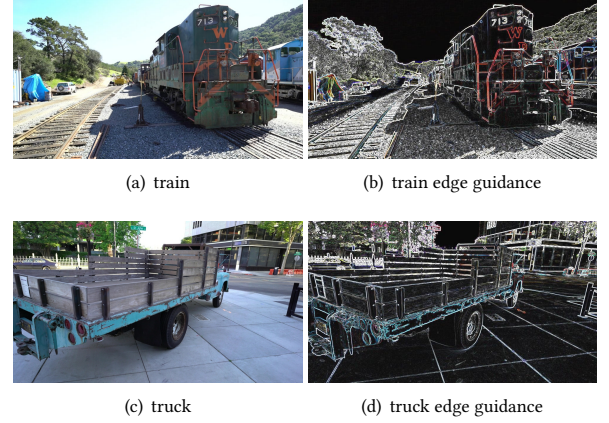


Figure 4: The edges guidance for the train and truck data set.

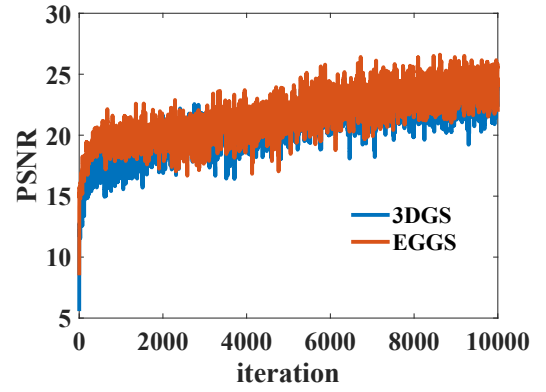


Figure 5: The PSNR during the training process (the lines are smoothed for better visualization). The blue line is 3DGS and the red line is EGGS. The proposed EGGS can achieve better results on the train data.

Table 1: The PSNR comparison of EGGS and 3DGS.

	Banana 3008 × 2000 16	Train 980 × 545 301	Truck 979 × 546 251
3DGS	41.7	28.0	28.4
EGGS	<b>43.8</b>	<b>29.2</b>	<b>29.5</b>
improved	2.1	1.2	1.1

The improvement might depend on several things, such as the input image number (view number), image resolution, the complexity of the 3D scene, the light condition, etc. The improvement in the banana data set is high because the input images have a high resolution and the scene has simple geometry. Most of the edge guidance is on the banana itself. In contrast, the edge guidance in the train and truck data set contains the trees and buildings, which might hamper the edge guidance.



## 4 CONCLUSION

In this paper, we present a simple yet effective edge guidance for the Gaussian splatting method. The proposed edge guidance is only determined by the multi view input images. And thus it does not increase the computation cost during the training and rendering stage in the Gaussian splatting method. Moreover, as shown in the experiments, this edge guidance can improve the accuracy of the radian field about  $1 \sim 2$  dB.

The proposed edge guidance forces the Gaussian particles to be aligned with the edges in the scene. Therefore, it will help in improving the accuracy of geometry representation [8, 9, 21].

The proposed edge guided Gaussian splatting method can achieve higher accuracy for the scene representation and rendering. It can be applied in a large range of applications where edge information is important [5–7, 10–20, 22, 31, 35–39, 41].

## ACKNOWLEDGMENTS

This work was supported by National Natural Science Foundation of China (61907031) and Shenzhen Science and Technology Program (20231121165649002 and JCYJ20220818100005011)

## REFERENCES

- [1] Rameen Abdal, Wang Yifan, Zifan Shi, Yinghao Xu, Ryan Po, Zhengfei Kuang, Qifeng Chen, Dit-Yan Yeung, and Gordon Wetzstein. 2023. Gaussian Shell Maps for Efficient 3D Human Generation. *arXiv:2311.17857* [cs.CV]
- [2] Guikun Chen and Wenguan Wang. 2024. A Survey on 3D Gaussian Splatting. *arXiv:2401.03890* [cs.CV]
- [3] Kai Cheng, Xiaoxiao Long, Kaizhi Yang, Yao Yao, Wei Yin, Yuexin Ma, Wenping Wang, and Xuejin Chen. 2024. GaussianPro: 3D Gaussian Splatting with Progressive Propagation. *arXiv:2402.14650* [cs.CV]
- [4] Zhiwen Fan, Kevin Wang, Kairun Wen, Zehao Zhu, Dejia Xu, and Zhangyang Wang. 2024. LightGaussian: Unbounded 3D Gaussian Compression with 15x Reduction and 200+ FPS. *arXiv:2311.17245* [cs.CV]
- [5] Yuanhao Gong. 2015. *Spectrally regularized surfaces*. Ph.D. Dissertation. ETH Zurich, Nr. 22616. <http://dx.doi.org/10.3929/ethz-a-010438292>.
- [6] Y. Gong. 2019. Mean Curvature Is a Good Regularization for Image Processing. *IEEE Transactions on Circuits and Systems for Video Technology* 29, 8 (Aug. 2019), 2205–2214. <https://doi.org/10.1109/TCSVT.2018.2866866>
- [7] Yuanhao Gong. 2022. Computing Curvature, Mean Curvature and Weighted Mean Curvature. *2022 IEEE International Conference on Image Processing (ICIP)*, 266–270. <https://doi.org/10.1109/ICIP46576.2022.9897816>
- [8] Yuanhao Gong. 2023. Imposing Total Variation Prior Into Guided Filter. In *Proc. IEEE Int. Conf. Image Processing (ICIP)*. 156–160. <https://doi.org/10.1109/ICIP49359.2023.10223111>
- [9] Yuanhao Gong. 2023. A Multiscale Residual Solver for Total Variation Models. In *Proc. IEEE Int. Conf. Image Processing (ICIP)*. 151–155. <https://doi.org/10.1109/ICIP49359.2023.10223111>
- [10] Yuanhao Gong. 2024. EGGS: Edge Guided Gaussian Splatting for Radiance Fields. *arXiv:2404.09105* [cs.CV]
- [11] Yuanhao Gong and Yong Chen. 2019. Computing Gaussian Curvature in Real-Time for 4K Video Processing. *IEEE Access* 7 (2019), 115936–115944. <https://doi.org/10.1109/ACCESS.2019.2936270>
- [12] Yuanhao Gong and Yong Chen. 2020. Molecular Surface Estimation by Geometric Coupled Distance Functions. *IEEE Access* 8 (2020), 176263–176273. <https://doi.org/10.1109/ACCESS.2020.3026757>
- [13] Yuanhao Gong and Orcun Goksel. 2019. Weighted mean curvature. *Signal Processing* 164 (2019), 329 – 339.
- [14] Yuanhao Gong, Xianxu Hou, Fei Li, and Guoping Qiu. 2018. Image Filtering With Generic Geometric Prior. *IEEE Access* 6 (2018), 54320–54330. <https://doi.org/10.1109/ACCESS.2018.2871829>
- [15] Y. Gong, B. Liu, X. Hou, and G. Qiu. 2018. Sub-window Box Filter. In *Proc. IEEE Visual Communications and Image Processing (VCIP)*. 1–4. <https://doi.org/10.1109/VCIP.2018.8698682>
- [16] Y. Gong, G. Paul, and I. F. Sbalzarini. 2012. Coupled signed-distance functions for implicit surface reconstruction. In *IEEE Intl. Symp. Biomed. Imaging (ISBI)*. 1000–1003. <https://doi.org/10.1109/ISBI.2012.6235726>
- [17] Yuanhao Gong and Ivo F. Sbalzarini. 2013. Local weighted Gaussian curvature for image processing. *Intl. Conf. Image Proc. (ICIP)* (September 2013), 534–538.
- [18] Yuanhao Gong and Ivo F. Sbalzarini. 2017. Curvature filters efficiently reduce certain variational energies. *IEEE Transactions on Image Processing* 26, 4 (April 2017), 1786–1798. <https://doi.org/10.1109/TIP.2017.2658954>
- [19] Yuanhao Gong, Wenming Tang, Lebin Zhou, Lantao Yu, and Guoping Qiu. 2021. A Discrete Scheme for Computing Image's Weighted Gaussian Curvature. In *2021 IEEE International Conference on Image Processing (ICIP)*. 1919–1923. <https://doi.org/10.1109/ICIP42928.2021.9506611>
- [20] Yuanhao Gong, Wenming Tang, Lebin Zhou, Lantao Yu, and Guoping Qiu. 2021. Quarter Laplacian Filter For Edge Aware Image Processing. In *Proc. IEEE Int. Conf. Image Processing (ICIP)*. 1959–1963. <https://doi.org/10.1109/ICIP42928.2021.9506503>
- [21] Yuanhao Gong, Qicong Wang, Chenhui Yang, Yahui Gao, and Cuihua Li. 2009. Symmetry Detection for Multi-object Using Local Polar Coordinate. *Lecture Notes in Computer Science* 5702 (2009), 277.
- [22] Y. Gong, H. Yin, J. Liu, B. Liu, and G. Qiu. 2019. Soft Tissue Removal in X-Ray Images by Half Window Dark Channel Prior. In *Proc. IEEE Int. Conf. Image Processing (ICIP)*. 3576–3580. <https://doi.org/10.1109/ICIP.2019.8803492>
- [23] Yuanhao Gong, Lantao Yu, and Guanghui Yue. 2024. Isotropic Gaussian Splatting for Real-Time Radiance Field Rendering. *arXiv:2403.14244* [cs.CV]
- [24] Antoine Guédon and Vincent Lepetit. 2023. SuGaR: Surface-Aligned Gaussian Splatting for Efficient 3D Mesh Reconstruction and High-Quality Mesh Rendering. *arXiv preprint arXiv:2311.12775* (2023).
- [25] Binbin Huang, Zehao Yu, Anpei Chen, Andreas Geiger, and Shenghua Gao. 2024. 2D Gaussian Splatting for Geometrically Accurate Radiance Fields. *arXiv:2403.17888* [cs.CV]
- [26] Junfeng Jing, Shenjuan Liu, Gang Wang, Weichuan Zhang, and Changming Sun. 2022. Recent advances on image edge detection: A comprehensive review. *Neurocomputing* 503 (2022), 259–271. <https://doi.org/10.1016/j.neucom.2022.06.083>
- [27] Bernhard Kerbl, Georgios Kopanas, Thomas Leimkuehler, and George Drettakis. 2023. 3D Gaussian Splatting for Real-Time Radiance Field Rendering. *ACM Trans. Graph.* 42, 4, Article 139 (jul 2023), 14 pages. <https://doi.org/10.1145/3592433>
- [28] Joo Chan Lee, Daniel Rho, Xiangyu Sun, Jong Hwan Ko, and Eunbyung Park. 2023. Compact 3D Gaussian Representation for Radiance Field. *arXiv preprint arXiv:2311.13681* (2023).
- [29] Yun Liu, Ming-Ming Cheng, Xiaowei Hu, Jia-Wang Bian, Le Zhang, Xiang Bai, and Jinhui Tang. 2019. Richer Convolutional Features for Edge Detection. *IEEE Transactions on Pattern Analysis and Machine Intelligence* 41, 8 (2019), 1939–1946. <https://doi.org/10.1109/TPAMI.2018.2878849>
- [30] Mengyang Pu, Yaping Huang, Yuming Liu, Qingji Guan, and Haibin Ling. 2022. EDTER: Edge Detection with Transformer. In *2022 IEEE/CVF Conference on Computer Vision and Pattern Recognition (CVPR)*. 1392–1402. <https://doi.org/10.1109/CVPR52688.2022.00146>
- [31] Wenming Tang, Yuanhao Gong, and Guoping Qiu. 2023. Feature preserving 3D mesh denoising with a Dense Local Graph Neural Network. 233 (2023), 103710. <https://doi.org/10.1016/j.cviu.2023.103710>
- [32] Jie Wang, Jiu-Cheng Xie, Xianyan Li, Feng Xu, Chi-Man Pun, and Hao Gao. 2024. GaussianHead: High-fidelity Head Avatars with Learnable Gaussian Derivation. *arXiv:2312.01632* [cs.CV]
- [33] Saining Xie and Zhuowen Tu. 2015. Holistically-Nested Edge Detection. In *2015 IEEE International Conference on Computer Vision (ICCV)*. 1395–1403. <https://doi.org/10.1109/ICCV.2015.164>
- [34] Yunzhi Yan, Haotong Lin, Chenxu Zhou, Weijie Wang, Haiyang Sun, Kun Zhan, Xianpeng Lang, Xiaowei Zhou, and Sida Peng. 2023. Street Gaussians for Modeling Dynamic Urban Scenes. (2023).
- [35] Hui Yin, Yuanhao Gong, and Guoping Qiu. 2019. Side Window Filtering. In *2019 IEEE/CVF Conference on Computer Vision and Pattern Recognition (CVPR)*. 8750–8758. <https://doi.org/10.1109/CVPR.2019.00896>
- [36] Hui Yin, Yuanhao Gong, and Guoping Qiu. 2019. Side window guided filtering. *Signal Process.* 165 (2019), 315–330. <https://doi.org/10.1016/j.sigpro.2019.07.026>
- [37] Hui Yin, Yuanhao Gong, and Guoping Qiu. 2020. Fast and efficient implementation of image filtering using a side window convolutional neural network. *Signal Process.* 176 (2020), 107717. <https://doi.org/10.1016/j.sigpro.2020.107717>
- [38] Lantao Yu, Dehong Liu, Hassan Mansour, and Petros T. Boufounos. 2022. Fast and High-Quality Blind Multi-Spectral Image Pansharpening. *IEEE Transactions on Geoscience and Remote Sensing* 60 (2022), 1–17. <https://doi.org/10.1109/TGRS.2021.3091329>
- [39] Lantao Yu and Michael T. Orchard. 2019. Single Image Interpolation Exploiting Semi-local Similarity. *ICASSP 2019 - 2019 IEEE International Conference on Acoustics, Speech and Signal Processing (ICASSP)*, 1722–1726. <https://doi.org/10.1109/ICASSP.2019.8682362>
- [40] Zhenglin Zhou, Fan Ma, Hehe Fan, and Yi Yang. 2024. HeadStudio: Text to Animatable Head Avatars with 3D Gaussian Splatting. *arXiv:2402.06149* [cs.CV]
- [41] Ming Zong, Ruili Wang, Xiubo Chen, Zhe Chen, and Yuanhao Gong. 2021. Motion saliency based multi-stream multiplier ResNets for action recognition. *Image and Vision Computing* 107 (2021), 104108.